

# Observational constraints on modified gravity models and cosmic topology

M.C. Bento,<sup>1,\*</sup> O. Bertolami,<sup>1,†</sup> M.J. Rebouças,<sup>2,‡</sup> and N.M.C. Santos<sup>3,§</sup>

<sup>1</sup>*Departamento de Física, Instituto Superior Técnico,  
Avenida Rovisco Pais, 1049-001 Lisboa, Portugal*

<sup>2</sup>*Centro Brasileiro de Pesquisas Físicas  
Rua Dr. Xavier Sigaud 150  
22290-180 Rio de Janeiro – RJ, Brazil*

<sup>3</sup>*Institut für Theoretische Physik, Universität Heidelberg  
Philosophenweg 16, 69120 Heidelberg, Germany*

(Dated: December 2, 2024)

We study the constraints that spatial topology may place on the parameters of models that account for the accelerated expansion of the universe via infrared modifications to general relativity, namely the Dvali-Gabadadze-Porrati braneworld model as well as the Dvali-Turner and Cardassian models. By considering the Poincaré dodecahedral space as the circles-in-the-sky observable spatial topology, we examine the constraints that can be placed on the parameters of each model using type Ia supernovae data together with the baryon acoustic peak in the large scale correlation function of the Sloan Digital Sky Survey of luminous red galaxies and the Cosmic Microwave Background Radiation shift parameter data. We show that knowledge of spatial topology does provide relevant constraints, particularly on the curvature parameter, for all models.

PACS numbers: 98.80.-k, 98.80.Es, 98.80.Jk, 95.36.+x

## I. INTRODUCTION

Models where gravity is modified by soft very long-range corrections, normally inspired in braneworld constructions, are an interesting approach to account for the recent accelerated expansion of the universe, with no need for dark energy. However, likewise the dark energy models, one expects the parameters of modified gravity models to be affected by the geometry of the universe. The description of the universe as a metrical manifold, requires the characterization of its geometry and its topology; hence, a key issue regarding our understanding of the universe concerns its 3-dimensional geometry and topology. Studies of the cosmic microwave background radiation (CMBR) such as the ones performed by the Wilkinson Microwave Anisotropy Probe (WMAP) allow for testing geometry, which is related with the intrinsic curvature of the 3-dimensional space. On the other hand, topology concerns global properties of space such as its shape and size and, clearly, 3-geometry restricts but does not determine the topology of its spatial section. However, in a locally spatially homogeneous and isotropic universe, the topology of its spatial sections determines the sign of its local curvature [1] and therefore dictates its geometry.

In the context of the standard Friedmann–Lemaître–Robertson–Walker (FLRW) cosmology, the universe is described by a space-time manifold  $\mathcal{M}_4$  which is decom-

posed into  $\mathcal{M}_4 = \mathbb{R} \times M_3$  and endowed with a locally (spatially) homogeneous and isotropic metric

$$ds^2 = -dt^2 + a^2(t) \left[ \frac{dr^2}{1 - kr^2} + r^2(d\theta^2 + \sin^2 \theta d\phi^2) \right], \quad (1)$$

where, depending on the sign of the constant spatial curvature  $k$ , the geometry of the 3-space  $M_3$  is either Euclidean ( $k = 0$ ), spherical ( $k = 1$ ), or hyperbolic ( $k = -1$ ).

Thus, since our 3-dimensional space  $M_3$  is chosen to be one of the following simply-connected spaces, Euclidean  $\mathbb{R}^3$ , spherical  $\mathbb{S}^3$ , or hyperbolic space  $\mathbb{H}^3$ , depending on the sign of the constant spatial curvature  $k$ , it is a common misconception that the Gaussian curvature  $k$  of  $M_3$  is all one needs to establish whether the 3-space where we live in is finite or not. However, it is known that the great majority of constant curvature 3-spaces,  $M_3$ , are multiply-connected quotient manifolds of the form  $\mathbb{R}^3/\Gamma$ ,  $\mathbb{S}^3/\Gamma$ , and  $\mathbb{H}^3/\Gamma$ , where  $\Gamma$  is a fixed-point free group of isometries of the corresponding covering space. Thus, for example, for the Euclidean geometry besides  $\mathbb{R}^3$  there are 6 classes of topologically distinct compact and orientable spaces  $M_3$  that can be endowed with this geometry, while for both the spherical and hyperbolic geometries there is an infinite number of non-homeomorphic (topologically inequivalent) manifolds with non-trivial topology that admit these geometries. On the other hand, since the ultimate spatial topology has not yet been determined by cosmological observations, our 3-dimensional space may be any of these possible quotient manifolds.

Quotient manifolds are compact in three independent directions, or compact in two or at least one independent direction. In compact manifolds, any two given points may be joined by more than one geodesic. Since the ra-

\*Electronic address: bento@sirius.ist.utl.pt; Also at CFTP, Instituto Superior Técnico, Avenida Rovisco Pais, 1049-001 Lisboa

†Electronic address: orfeu@cosmos.ist.utl.pt

‡Electronic address: reboucas@cbpf.br

§Electronic address: n.santos@thphys.uni-heidelberg.de

diation emitted by cosmic sources follows geodesics, the immediate observational consequence of a nontrivial detectable spatial non-trivial topology<sup>1</sup> of  $M_3$  is that there will be multiple images of either cosmic objects or specific spots on the CMBR. At very large scales, the existence of these multiple images (or pattern repetitions) is a physical effect that can be used to probe the 3-space topology.

Different strategies and methodologies have been devised to probe a putative non-trivial topology of the spatial sections of the universe (see, e.g. Refs. [3, 4] for reviews and details on cosmic crystallographic methods). For instance, the so-called circles-in-the-sky method, is based on the presence of multiple images of correlated circles in the CMBR maps [5]. In a space with a detectable non-trivial topology, the last scattering sphere (LSS) intersects some of its topological images along pairs of circles of equal radii, centered at different points on the LSS, with the same distribution of temperature fluctuations,  $\delta T$ . These pairs of matching circles will be imprinted on the CMBR anisotropy sky maps regardless of the background geometry or detectable topology [5, 6]. Hence, it follows that in order to probe observationally a non-trivial topology, one should examine the full-sky CMBR maps in order to extract the correlated circles, and use their angular radii and the relative position of their centers to probe a putative non-trivial topology of the spatial sections of the observable universe.

In this regard, the Poincaré dodecahedral space [7] has been recently considered as the observable spatial topology of the universe in order to reanalyze the current type Ia supernovae (SNe Ia) as well as SNe Ia plus X-ray gas mass fraction constraints on the density parameters associated with dark matter ( $\Omega_m$ ) and dark energy ( $\Omega_\Lambda$ ) in the context of the  $\Lambda$ CDM model [8]. It was shown that the Poincaré dodecahedral space topology through the circles-in-the-sky method yields stringent constraints on the energy density parameters allowed by these observational data sets, reducing degeneracies considerably.

More recently, the circles-in-the-sky method has been used to place constraints on the parameters of the generalized Chaplygin gas (GCG) model [9, 10, 11], as discussed in Ref. [12]. In that work, by using both the Poincaré dodecahedral and binary octahedral topologies, it has been shown that these spatial topologies through circles-in-the-sky do provide additional constraints on the  $A_s$  parameter of the GCG model as allowed by the SNe Ia observations.

Given these encouraging results it is natural to use this strategy to constrain the parameters of modified gravity models as well. We will address this issue in the context of the following brane inspired modifications to gravity: the Dvali-Gabadze-Porrati [13] (DGP) model, as generalized to cosmology in Ref. [14] as well as the Dvali-

Turner [15] and Cardassian [16] models. To this end, we use the Poincaré dodecahedral space topology<sup>2</sup> to reanalyze current constraints on the parameters of these models, as provided by the so-called *gold* sample of 157 SNe Ia [21], as well as the baryon oscillation acoustic peak in the large scale correlation function of the Sloan Digital Sky Survey (SDSS) [22] and the CMBR shift parameter [23].

## II. MODIFIED-GRAVITY MODELS

Modified gravity models explore the possibility that there is no dark energy, and consider instead that infrared modifications to general relativity exist on very large scales, accounting in this way for the observed late time acceleration of the universe.

### A. Dvali-Gabadaze-Porrati model

One of the simplest covariant modified-gravity models is based on the DGP braneworld model [13], as generalized in Ref. [14] to a FLRW brane in a Minkowski bulk.

In the DGP model, standard model gauge fields are confined to a (3+1)D brane residing in an non-compact (4+1)D bulk, with different scales of gravity on the brane and in the bulk. The gravitational part of the action is given by

$$S = \frac{M_5^3}{2} \int d^4x dw \sqrt{g^{(5)}} R_5 + \frac{M_{Pl}^2}{2} \int d^4x \sqrt{g} R_4, \quad (2)$$

where  $M_5$  denotes the 5D Planck mass,  $M_{Pl}$  is the 4D Planck mass,  $g^{(5)}$  is the trace of the 5D metric  $g_{AB}^{(5)}$  ( $A, B = 0, 1, 2, \dots, 4$ ),  $w$  is the extra spatial coordinate,  $g$  the trace of the 4D metric induced in the brane,  $g_{\mu\nu}(x) \equiv g_{\mu\nu}^{(5)}(x, w = 0)$ , and where  $R_5$ ,  $R_4$  are the 5D and 4D scalar curvatures, respectively. This gravitational action coupled to matter on the brane leads to a modified Friedmann equation, which can be written as [14]

$$H^2 + \frac{k}{a^2} = \left( \sqrt{\frac{8\pi\rho}{3M_{Pl}^2}} + \frac{1}{4r_c^2} + \frac{1}{2r_c} \right)^2, \quad (3)$$

where

$$r_c = \frac{M_{Pl}^2}{2M_5^3} \quad (4)$$

<sup>1</sup> The extent to which a non-trivial topology may be detected was discussed in Refs. [2].

<sup>2</sup> It is worth remarking that this spatial topology accounts for the low value of the CMBR quadrupole and octopole moments measured by first year WMAP data [17], which has been confirmed by the most recent WMAP data analysis [18], and fits the temperature two-point correlation function [7, 19, 20].

is a length scale beyond which gravity starts to leak out into the bulk.

Rewriting the above equation in dimensionless variables  $\Omega_x = \rho_x/\rho_{crit}$  with  $\rho_{crit} = 3 M_{Pl}^2 H_0^2/8\pi$  and  $\rho_x$  the energy density in the component  $x$  today, we get

$$\left(\frac{H}{H_0}\right)^2 = \Omega_k(1+z)^2 + \left(\sqrt{\Omega_m(1+z)^3 + \Omega_{r_c}} + \sqrt{\Omega_{r_c}}\right)^2, \quad (5)$$

where  $H_0$  is the Hubble expansion parameter today and  $z$  is the redshift, and we have taken into account that, at present, the universe is matter dominated, hence  $\rho \simeq \rho_m$ . Moreover,  $\Omega_k = -\frac{k}{a_0^2 H_0^2}$  is the present curvature parameter and

$$\sqrt{\Omega_{r_c}} = \frac{1}{2r_c H_0}. \quad (6)$$

The constraint equation between the various components of energy density at  $z = 0$  is then given by

$$\Omega_k + \left(\sqrt{\Omega_{r_c} + \Omega_m} + \sqrt{\Omega_{r_c}}\right)^2 = 1. \quad (7)$$

It has been shown that the observed recent acceleration of the universe can be obtained from the extra contribution to the Friedmann equation by setting the length scale  $r_c$  close to the horizon size [24, 25].

## B. Dvali-Turner model

Inspired in the above construction, Dvali and Turner considered a more generic modification of the Friedmann equation [15], hereafter referred to as DT model

$$H^2 + \frac{k}{a^2} = \frac{8\pi\rho}{3M_{Pl}^2} + \frac{1}{r_c^{2-\beta}} \left(H^2 + \frac{k}{a^2}\right)^{\beta/2}. \quad (8)$$

Notice that  $\beta$  is the only parameter of the model: the case  $\beta = 1$  corresponds to the DGP model,  $\beta = 0$  to the cosmological constant case, and  $\beta = 2$  to a “renormalization” of the Friedmann equation. A stringent bound follows from requiring that the new term does not interfere with the formation of large-scale structure,  $\beta \leq 1$ , whereas the successful predictions of Big-Bang nucleosynthesis impose a weaker limit on  $\beta$ , namely,  $\beta \leq 1.95$ . Moreover, it can be shown that this correction behaves like dark energy in the recent past, with equation of state  $w_{eff} = -1 + \beta/2$ , and  $w = -1$  in the distant future; moreover, it can mimic  $w < -1$  without violating the weak-energy condition [15].

The expression for the Hubble expansion as a function of redshift is then

$$\left(\frac{H}{H_0}\right)^2 - 2\sqrt{\Omega_{r_c}} \left[ \left(\frac{H}{H_0}\right)^2 - \Omega_k(1+z)^2 \right]^{\beta/2} = \Omega_m(1+z)^3 + \Omega_k(1+z)^2, \quad (9)$$

where  $\Omega_{r_c}$  is now generalized to

$$\sqrt{\Omega_{r_c}} = \frac{1}{2(r_c H_0)^{2-\beta}}, \quad (10)$$

which means that the constraint between the various densities at  $z = 0$  is given by

$$\Omega_m + \Omega_k + 2\sqrt{\Omega_{r_c}}(1 - \Omega_k)^{\beta/2} = 1. \quad (11)$$

## C. Cardassian model

We will also consider the so called Cardassian model [16], which explains the current acceleration of the universe by a modification of the Friedmann equation consisting basically in the introduction of an additional term proportional to  $\rho^n$

$$H^2 = \frac{8\pi}{3M_{Pl}^2} (\rho + b\rho^n) - \frac{k}{a^2}, \quad (12)$$

where  $b$  and  $n$  are constants, and we have added a curvature term to the original Cardassian model. As in the previous cases, in this model the universe is composed only of radiation and matter (including baryon and cold dark matter) and the energy density required to close the universe is much smaller than in standard cosmology, so that matter can be sufficient to provide a flat (or close to flat) geometry.

For  $n < 1$  the second term becomes important if  $z < \mathcal{O}(1)$ ; thereon it dominates the Friedmann equation and yields  $a \propto t^{2/3n}$  for ordinary matter, so acceleration will occur provided  $n < 2/3$ . There are two main motivations for the introduction of the extra term, namely terms of that form typically when the universe is embedded as a three-dimensional surface (3-brane) in higher dimensions [26] or, alternatively, it may appear in a purely 4D theory due to an extra contribution to the total energy density as would be the case if there were some unknown interactions between matter particles [27].

In a matter dominated universe, Eq. (12) can be rewritten as

$$\left(\frac{H}{H_0}\right)^2 = \Omega_m(1+z)^3 + \Omega_k(1+z)^2 + (1 - \Omega_m - \Omega_k)(1+z)^{3n}. \quad (13)$$

Notice that the case  $n = 0$  corresponds to the  $\Lambda$ CDM model.

Finally, it is worth pointing out that these models have been thoroughly scrutinized from the observational point of view using constraints from CMBR, SNe Ia and large scale structure. For recent studies see, for instance, Refs. [28, 29, 30, 31, 32, 33, 34, 35, 36].

## III. COSMIC TOPOLOGY IN BRANE COSMOLOGY

In the context of the 5D braneworld models the universe is described by a 5-dimensional metrical orbifold

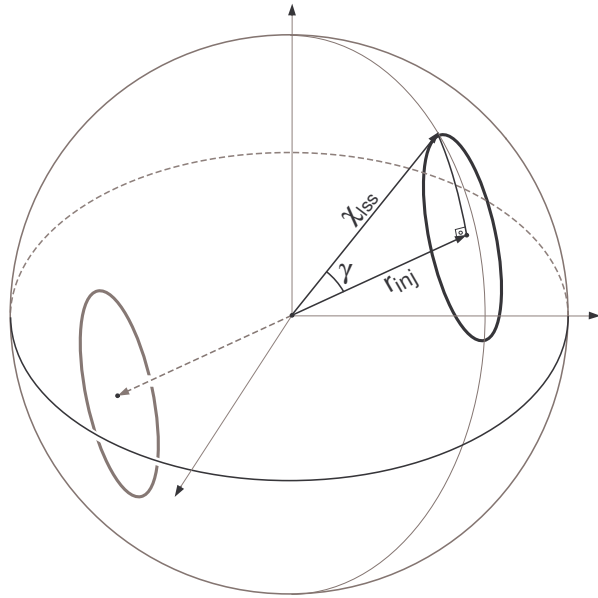


FIG. 1: A schematic illustration of two antipodal matching circles in the LSS. These pair of circles come about in all globally homogeneous positively curved manifolds with a circles-in-the-sky detectable topology. The relation between the angular radius  $\gamma$ , angular sides  $r_{inj}$  and  $\chi_{lss}$  is given by the following Napier's rule for spherical triangles,  $\cos \gamma = \tan r_{inj} \cot \chi_{lss}$ .

(bulk)  $\mathcal{O}_5$  that is mirror symmetric ( $\mathbb{Z}_2$ ) across the 4D brane (manifold)  $\mathcal{M}_4$ . Thus, the bulk can be decomposed as  $\mathcal{O}_5 = \mathcal{M}_4 \times E_1 = \mathbb{R} \times M_3 \times E_1$ , where  $E_1$  is a  $\mathbb{Z}_2$  symmetric Euclidean space, and where  $\mathcal{M}_4$  is endowed with a Robertson–Walker metric Eq. (1), which is recovered when  $w = 0$  for the extra non-compact dimension. In this way, the multiplicity of possible inequivalent topologies of our 3-dimensional space, and the physical consequences of a non-trivial detectable topology of  $M_3$  (possible multiple images of discrete cosmic sources, circle-in-the-sky on the LSS) is brought on the braneworld scenario.

### A. Poincaré Dodecahedral Space Model

The Poincaré dodecahedral space  $\mathcal{D}$  is a 3-manifold of the form  $\mathbb{S}^3/\Gamma$  in which  $\Gamma = I^*$  is the binary icosahedral group of order 120. It is represented by a regular spherical dodecahedron (12 pentagonal faces) along with the identification of the opposite faces after a twist of  $36^\circ$ . Such a space is positively curved ( $k=1, \Omega_k < 0$ ), and tiles the 3-sphere  $\mathbb{S}^3$  into 120 identical spherical dodecahedra.

The observed values of the power measured by WMAP of the CMBR quadrupole ( $\ell = 2$ ) and octopole ( $\ell = 3$ ) moments, and the sign of the curvature density  $\Omega_k = -0.02 \pm 0.02$  reported by first year WMAP data analysis team [17], which has been reinforced by the three-year WMAP observations (cf. Table 11 of Ref. [18]),

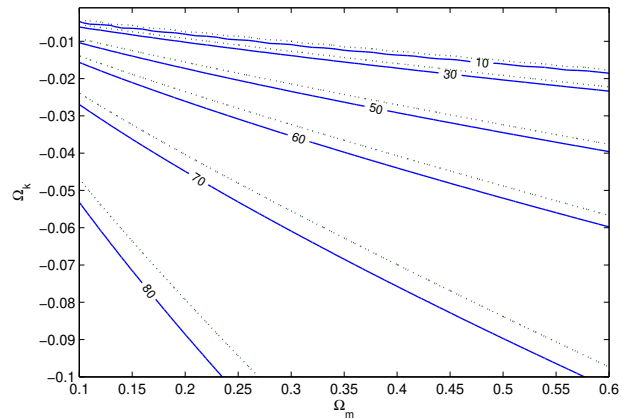


FIG. 2: Lines of constant angular radius,  $\gamma$ , in the  $\Omega_k - \Omega_m$  plane for the DGP (solid) and  $\Lambda$ CDM (dashed) models.

have motivated the suggestion of the Poincaré dodecahedral space topology as an explanation for this observed large-angle anomaly in the CMB power spectrum [7]. This observation has sparked the interest in the dodecahedral space, which has been examined on its various features [19, 20, 37, 38, 39]. Therefore, it turns out that a universe with the Poincaré dodecahedral space section squares with WMAP data in that it accounts for the suppression of power at large angle observed by WMAP [17, 18], and fits the WMAP temperature two-point correlation function [19, 20], retaining the standard FLRW background for local physics.

Notice that a preliminary search of the antipodal matched circles in the WMAP sky maps predicted by the Poincaré model has failed [37]. A second search of the correlated circles for the  $\mathcal{D}$  space was not conclusive either [40]. This absence of evidence of correlated circles may be due to several causes, such as the Sunyaev–Zeldovich effect, lensing and the finite thickness of the LSS, as well as possible systematics in the removal of the foregrounds, which can damage the topological circle matching. Thus, it is conceivable that the correlated circles may have been overlooked in the CMBR sky maps search [19].

### B. The Circles-in-the-Sky Method

An important class of constant curvature positively-curved 3-spaces with a non-trivial topology is comprised by the *globally homogeneous* manifolds. These manifolds satisfy the topological principle of (global) homogeneity, in the sense that all points in  $M_3$  are topologically equivalent. In particular, in these spaces the pairs of matching circles will be antipodal, as shown in Figure 1.

The Poincaré dodecahedral space  $\mathcal{D}$  is globally homogeneous, and give rise to six pairs of antipodal matched

Model	Parameters	SN	SN+SDSS	SN+SDSS+CMBR	SN+SDSS+CMBR+T
$\Lambda$ CDM	$\Omega_m$	0.46	0.28	0.28	0.29
	$\Omega_k$	-0.44	0.033	-0.003	-0.020
	$\chi^2$	181.24	183.76	183.93	184.44
DGP	$\Omega_m$	0.33	0.27	0.27	0.28
	$\Omega_k$	-0.56	-0.32	0.014	-0.021
	$\chi^2$	181.36	182.04	190.53	192.34
DT	$\beta$	-10	1.0	0.26	0.23
	$\Omega_m$	0.49	0.27	0.28	0.29
	$\Omega_k$	0.032	-0.32	-0.002	-0.02
	$\chi^2$	180.55	182.04	183.54	184.11
Card	$n$	-6.15	0.33	0.042	0.041
	$\Omega_m$	0.33	0.27	0.28	0.29
	$\Omega_k$	0.33	-0.76	-0.003	-0.020
	$\chi^2$	178.77	182.08	183.72	184.23

TABLE I: Best fit parameters for the  $\Lambda$ CDM, DGP, DT and Cardassian models for different combinations of observational constraints (SN = SNe Ia gold sample, SDSS = SDSS baryon acoustic oscillations, CMBR = CMBR shift parameter and T =Poincaré dodecahedral space topology for  $\gamma = 50^\circ \pm 6^\circ$ ).

circles on the LSS, centered in a symmetrical pattern as the centers of the faces of the dodecahedron. Figure 1 shows a pair of these antipodal circles. Clearly the distance between the centers of each pair of these correlated circles is twice the radius  $r_{inj}$  of the sphere inscribed in  $\mathcal{D}$ .

It then follows from the use of trigonometric relations (known as Napier's rules) for the right-angled spherical triangle shown in Fig. 1 gives origin to a relation between the angular radius  $\gamma$ , the angular sides  $r_{inj}$  and radius  $\chi_{lss}$  of the LSS, namely

$$\chi_{lss} = \tan^{-1} \left[ \frac{\tan r_{inj}}{\cos \gamma} \right], \quad (14)$$

where  $r_{inj}$  is a topological invariant, equal to  $\pi/10$  for the the space  $\mathcal{D}$ , and the distance  $\chi_{lss}$  to the origin is given by

$$\chi_{lss} = y(z_{lss}), \quad (15)$$

where  $z_{lss} = 1089$  [17] and we have defined a new function

$$y(z) \equiv \sqrt{|\Omega_k|} \int_0^z \frac{H_0}{H(z')} dz'. \quad (16)$$

Eq. (15) makes apparent that  $\chi_{lss}$  depends on the cosmological scenario. Moreover, Eq. (14) with  $\chi_{lss}$  given by Eq. (15) together with the ratio  $H_0/H$  for each modified-gravity model yield a relation between the angular radius  $\gamma$  and the cosmological parameters of each model. Thus, they can be used to set bounds (confidence regions) on model parameters. To quantify this, we consider a typical angular radius  $\gamma = 50^\circ$  estimated in Ref. [19] for the Poincaré dodecahedral space and, since the measurements of the radius  $\gamma$  do involve observational uncertainties on the model parameters from the detection of the

spatial topology, we take into account these uncertainties; in order to obtain conservative results, we consider  $\delta\gamma \simeq 6^\circ$ , which is the scale below which the circles are blurred for the Poincaré dodecahedral space case [19].

In Fig. 2 we show how our results regarding the DGP and  $\Lambda$ CDM models depend on the angular radius,  $\gamma$ . This figure displays the lines of constant  $\gamma$  in the  $\Omega_k - \Omega_m$  plane for these models. We see that when the angular radius increases  $\Omega_k$  becomes more negative and that, for any given value of the angular radius, the  $\Lambda$ CDM model prefers a less curved universe as compared with the DGP model. It is also clear that the bounds of topological origin on  $\Omega_k$  are expected to be very similar for both models, for any given angular radius in the interval  $60^\circ \lesssim \gamma \lesssim 10^\circ$ ; however, for  $\gamma \gtrsim 70^\circ$  the distinction between these bounds for the  $\Lambda$ CDM and DGP models becomes more important. Finally, any additional constraints from topology on  $\Omega_m$  are expected to be very weak unless  $\gamma > 70^\circ$ .

## IV. OBSERVATIONAL CONSTRAINTS

### A. Constraints from SNe Ia

For our analysis, we consider the set of SNe Ia data recently compiled by Riess *et al.* [21] known as the *gold* sample. This set contains 157 points: 143 points taken from the 230 Tonry *et al.* [41] data plus 23 points from Barris *et al.* [42] and 14 points discovered using HST [21]. Various points where the classification of the supernovae was uncertain or the photometry was incomplete have been discarded, thus increasing the reliability of the sample. The data points in the *gold* sample are given in terms

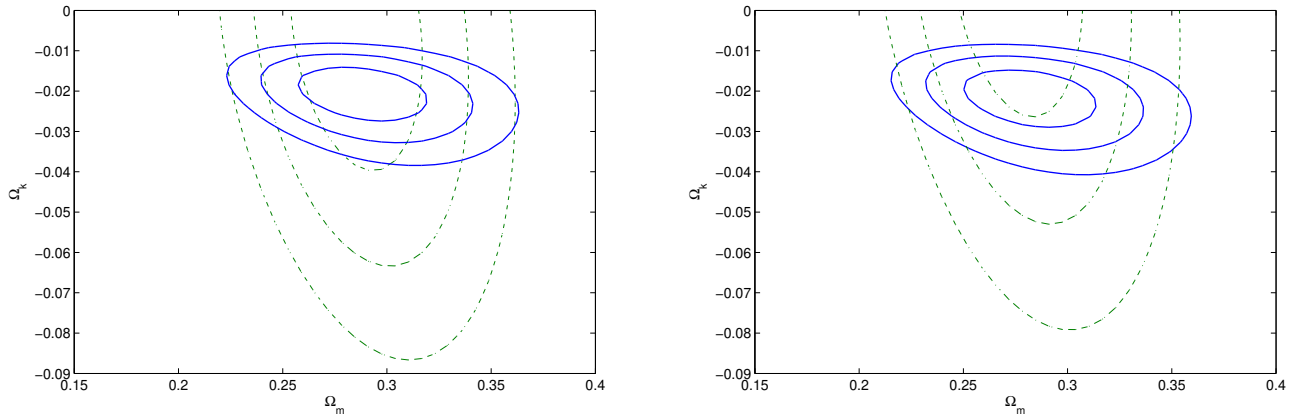


FIG. 3: Confidence contours (68.3%, 95.4% and 99.7%) in the  $\Omega_m - \Omega_k$  plane for the  $\Lambda$ CDM (left) and DGP (right) models obtained with the SNe Ia gold sample plus the SDSS acoustic peak data and CMBR shift parameter assuming a  $\mathcal{D}$  space topology with  $\gamma = 50^\circ \pm 6^\circ$ . Also shown are the contours obtained without the constraint from cosmic topology (dashed lines).

of the distance modulus

$$\mu_{\text{obs}}(z) \equiv m(z) - M_{\text{obs}}(z) , \quad (17)$$

and the respective errors  $\sigma_{\mu_{\text{obs}}}(z)$ , which already take into account the effects of peculiar motions. The apparent magnitude  $m$  is related to the dimensionless luminosity distance

$$D_L(z) = \frac{1+z}{\sqrt{|\Omega_k|}} S(y(z)) , \quad (18)$$

where  $S(x) \equiv (\sin(x), \sinh(x), x)$  for  $\Omega_k < 0$ ,  $\Omega_k > 0$  and  $\Omega_k = 0$ , respectively, by

$$m(z) = \mathcal{M} + 5 \log_{10} D_L(z) . \quad (19)$$

The  $\chi^2$  is calculated from

$$\chi_{SN}^2 = \sum_{i=1}^n \left[ \frac{\mu_{\text{obs}}(z_i) - \mathcal{M}' - 5 \log_{10} D_{L\text{th}}(z_i; \alpha_i)}{\sigma_{\mu_{\text{obs}}}(z_i)} \right]^2 , \quad (20)$$

where  $\mathcal{M}' = \mathcal{M} - M_{\text{obs}}$  is a nuisance parameter,  $\alpha_i$  are the model parameters and  $D_{L\text{th}}(z; \alpha_i)$  is the theoretical prediction for the dimensionless luminosity distance determined using the modified Friedmann equations.

## B. Constraints from the SDSS baryon acoustic oscillations

In order to further remove degeneracies intrinsic to the distance fitting methods, it is interesting to consider also the effect of the baryon acoustic peak of the large scale correlation function at  $100h^{-1}$  Mpc separation, detected by the SDSS team using a sample of LRG [22]. The

position of the acoustic peak is related to the quantity

$$\mathcal{A} = \sqrt{\Omega_m} \left( \frac{H_0}{H(z_{lrg})} \right)^{1/3} \left[ \frac{1}{z_{lrg} \sqrt{|\Omega_k|}} \mathcal{S}(y(z_{lrg})) \right]^{2/3} , \quad (21)$$

which takes the value  $\mathcal{A}_0 = 0.469 \pm 0.017$ , and where  $z_{lrg} = 0.35$  [22]. We have neglected the weak dependence of  $\mathcal{A}_0$  on the spectral tilt. The baryon acoustic peak is taken into account by adding the term

$$\chi_{sdss}^2 = \left( \frac{\mathcal{A}_0 - \mathcal{A}}{\sigma_{\mathcal{A}}} \right)^2 \quad (22)$$

to the  $\chi^2$ , where  $\sigma_{\mathcal{A}}$  is the error of  $\mathcal{A}_0$ .

We should point out that there is a level of uncertainty regarding baryon oscillations in the measurement of  $\mathcal{A}$  due to uncertainties essentially on  $\Omega_m$  (notice that uncertainties on the baryon density  $\Omega_b$  are constrained by the CMBR and Big Bang nucleosynthesis to be smaller than about 2%). Also, one should notice that the baryon acoustic oscillations were analyzed using a fiducial  $\Lambda$ CDM model and the full data set was compressed to a constraint at a single redshift [22]. As pointed out by Dick *et al* [43], the reduction of the data was intended to be valid for the case of a  $\Lambda$ CDM model, and robust against changes in a constant equation of state, but may give rise to significant systematic errors for the models we are considering.

## C. Constraints from the CMBR shift parameter

It is expected that when the cosmological parameters are varied, there is a shift in the whole CMBR angular spectrum, that is  $\ell \rightarrow \mathcal{R}\ell$ , with the shift parameter  $\mathcal{R}$

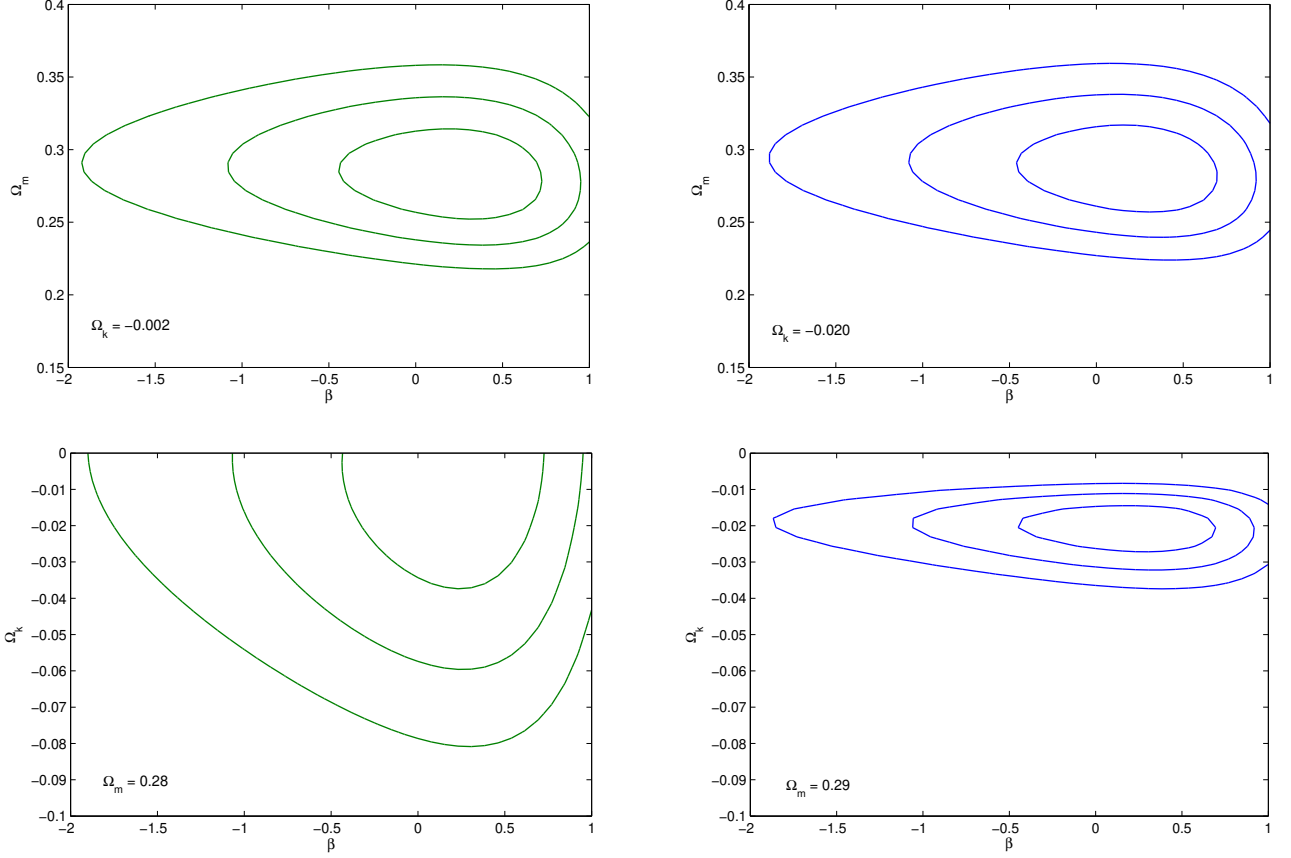


FIG. 4: Confidence contours (68.3%, 95.4% and 99.7%) for the DT model, in the  $\Omega_m - \beta$  (top) and  $\Omega_k - \beta$  (bottom) planes, obtained with the SN + SDSS + CMB data (left) and including also a  $\mathcal{D}$  space topology with  $\gamma = 50^\circ \pm 6^\circ$  (right).  $\Omega_k$  or  $\Omega_m$  are fixed at the value that minimizes the  $\chi^2$ .

being given by [23]

$$\mathcal{R} = \sqrt{\frac{\Omega_m}{|\Omega_k|}} S(y(z_{lss})) . \quad (23)$$

The results from CMBR (WMAP, CBI, ACBAR) data correspond to  $\mathcal{R}_0 = 1.716 \pm 0.062$  (using results from Spergel et al. [17]). We include the CMBR data in our analysis by adding

$$\chi^2_{cmb} = \left( \frac{\mathcal{R}_0 - \mathcal{R}}{\sigma_{\mathcal{R}}} \right)^2 , \quad (24)$$

to the total  $\chi^2$  function, where  $\mathcal{R}$  is computed for each model using Eq. (23).

#### D. Constraints from cosmic topology

The effect of cosmic topology is taken into account by adding a new term to the  $\chi^2$  as

$$\chi^2_{top} = \left( \frac{\chi_{lss} - \chi_{lss}^{\text{th}}}{\sigma_{\chi_{lss}}} \right)^2 . \quad (25)$$

The value of  $\chi_{lss}$  is given by Eq. (15) and the uncertainty  $\sigma_{\chi_{lss}}$  comes from the uncertainty  $\delta\gamma$  of the circles-in-the-sky method. The theoretical value of  $\chi_{lss}$  for each model is obtained from  $\chi_{lss} = y(z_{lss})$  combined with the respective expansion law.

## V. RESULTS

We have performed a best fit analysis with the minimization of the total  $\chi^2$ ,

$$\chi^2 = \chi^2_{SN} + \chi^2_{sdss} + \chi^2_{cmb} + \chi^2_{top} , \quad (26)$$

for the modified gravity models mentioned above using a MINUIT [44] based code. Notice that we marginalize analytically over  $\mathcal{M}'$  and that we allow the parameters  $\beta$  and  $n$  to vary in the interval  $[-10, 1]$  and  $[-10, 2/3]$ , respectively. Since the Poincaré dodecahedral space is positively curved, in the cases where topology is taken into account, we use the prior  $\Omega_k < 0$ . Our results are summarized in Table I.

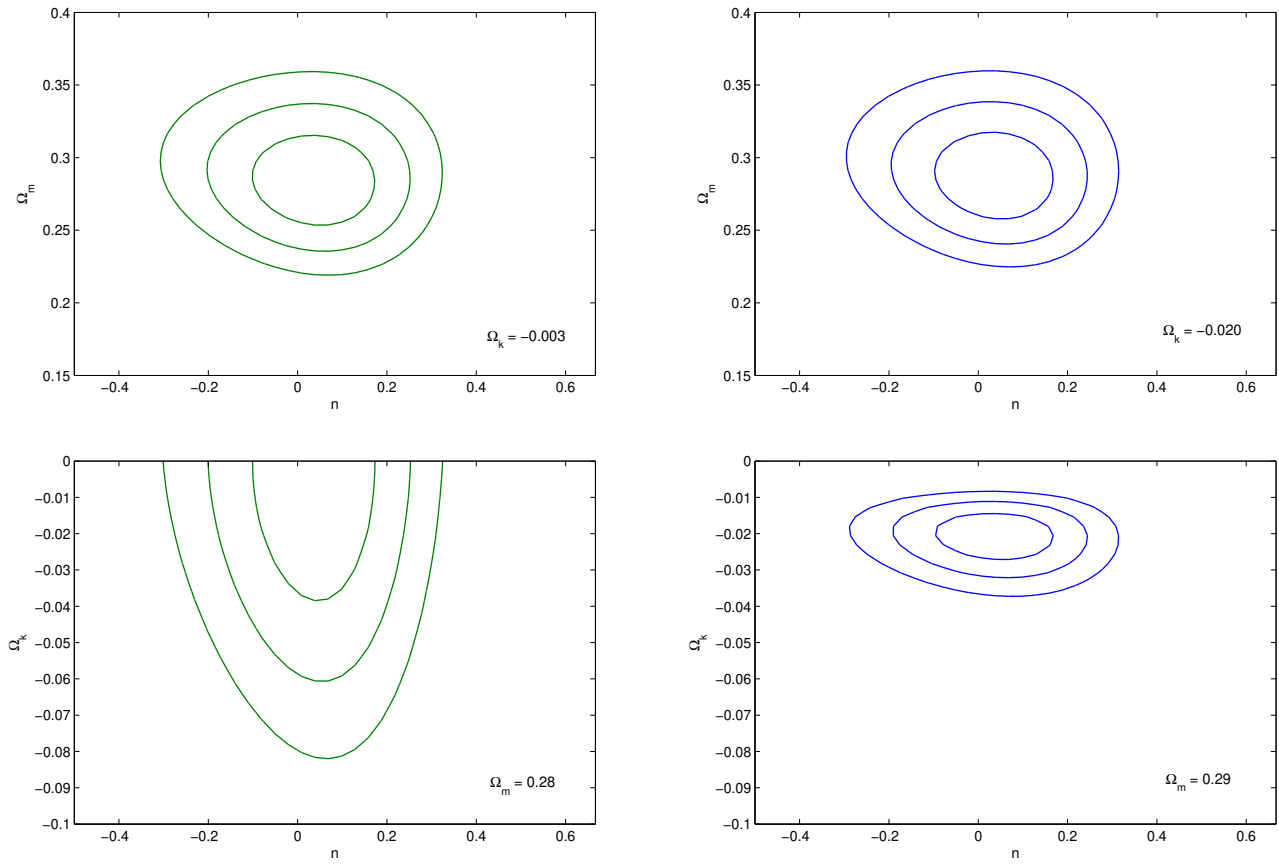


FIG. 5: Confidence contours (68.3%, 95.4% and 99.7%) for the Cardassian model, in the  $\Omega_m - n$  (top) and  $\Omega_k - n$  (bottom) planes, obtained with the SN + SDSS + CMB data (left) and including also a  $\mathcal{D}$  space topology with  $\gamma = 50^\circ \pm 6^\circ$  (right).  $\Omega_k$  or  $\Omega_m$  are fixed at the value that minimizes the  $\chi^2$ .

In Fig. 3, we show the 1, 2 and 3  $\sigma$  confidence contours in the  $\Omega_m - \Omega_k$  plane for the  $\Lambda$ CDM (left) and DGP (right) models obtained using the SNe Ia gold sample, SDSS acoustic peak and CMBR shift parameter data, assuming a  $\mathcal{D}$  space topology with  $\gamma = 50^\circ \pm 6^\circ$ . We also show the contours obtained without the constraint from cosmic topology (dashed lines). We see that the effect of including the topology constraint leads to a reduction of degeneracies, which is particularly relevant for the curvature parameter,  $\Omega_k$ .

It is also clear from Table I that the effect of the CMBR shift parameter is to push the best fit values for  $\Omega_k$  towards a flat universe, while the SDSS baryon oscillation data constrains  $\Omega_m$ , in agreement with the results of Refs. [34, 35, 36].

Our results for the DT and Cardassian models are shown in Figs. 4 and 5. For these models, again the effect of topology is clearly important for the curvature parameter,  $\Omega_k$ , and does not affect significantly the remaining parameters.

We have checked that, although the best fit for  $\Omega_k$  changes for different values of the angular radius,  $\gamma$ , this

dependence is not very strong (see Fig. 2). For instance, if we assume a smaller value for  $\gamma$ , e.g.  $\gamma = 11^\circ \pm 1^\circ$ , as suggested in Ref. [38], the allowed regions will be shifted slightly towards values of  $\Omega_k$  closer to 0. On the other hand, changes in the uncertainty of the angular radius alter the area corresponding to the confidence regions.

## VI. CONCLUSIONS

In general relativity, as well as in any metrical theory of gravitation of some generality and scope, a common approach to cosmological modelling commences with a space-time manifold endowed with a Lorentzian metric. The metrical approach to modelling the physical world has often led physicists to restrict their studies to the purely geometric features of space-time, either by ignoring the role of spatial topology or by considering just the simply-connected topological alternatives. However, since the topological properties of a manifold are more fundamental than its metrical features, it is important to determine to what extent physical results related to

a FLRW universe are constrained by the topology of its spatial section.

The so-called circles-in-the-sky method makes apparent that a non-trivial detectable topology of the spatial section of the universe is an observable attribute, and can be probed for any locally spatially homogeneous and isotropic space.

By assuming the Poincaré dodecahedral space  $\mathcal{D}$  as the circles-in-the-sky detected topology of the spatial sections of the universe, we have re-analyzed the current constraints on the parameters of three modified gravity models that account for the accelerated expansion of the universe via long-range corrections to the Friedmann equation. To this end, we have used the gold dataset of SNe Ia, the results of the SDSS galaxy survey for the baryon acoustic peak in the large scale correlation function and the WMAP results for the CMBR shift parameter

together with the circles-in-the-sky method for the  $\mathcal{D}$  topology.

The main outcome of our analysis is that the knowledge of the spatial topology of the Universe through the circles-in-the-sky method yields important additional constraints on the curvature parameter for the models we have considered.

## Acknowledgments

M.J.R thanks CNPq for the grant under which this work was carried out, and is grateful to J.S. Alcaniz for useful discussions. The work of M.C.B. and O. B. was supported by Fundação para a Ciência e a Tecnologia (FCT, Portugal) under the grant POCI/FIS/56093/2004.

---

[1] I.N. Bernshtein and V.F. Shvartsman, Sov. Phys. JETP **52**, 814 (1980).

[2] G.I. Gomero, M.J. Rebouças, and R. Tavakol, Class. Quantum Grav. **18**, 4461 (2001); G.I. Gomero, M.J. Rebouças, and R. Tavakol, Class. Quantum Grav. **18**, L145 (2001); G.I. Gomero, M.J. Rebouças, and R. Tavakol, Int. J. Mod. Phys. A **17**, 4261 (2002); J.R. Weeks, R. Lehoucq, and J.-P. Uzan, Class. Quantum Grav. **20**, 1529 (2003); J.R. Weeks, Mod. Phys. Lett. A **18**, 2099 (2003); G.I. Gomero and M.J. Rebouças, Phys. Lett. A **311**, 319 (2003); B. Mota, M.J. Rebouças, and R. Tavakol, Class. Quantum Grav. **20**, 4837 (2003).

[3] M. Lachièze-Rey and J.-P. Luminet, Phys. Rep. **254**, 135 (1995); G.D. Starkman, Class. Quantum Grav. **15**, 2529 (1998); J. Levin, Phys. Rep. **365**, 251 (2002); M.J. Rebouças and G.I. Gomero, Braz. J. Phys. **34**, 1358 (2004), astro-ph/0402324; M.J. Rebouças, astro-ph/0504365.

[4] R. Lehoucq, M. Lachièze-Rey, and J.-P. Luminet, Astron. Astrophys. **313**, 339 (1996); B.F. Roukema, Class. Quantum Grav. **15**, 2645 (1998); R. Lehoucq, J.-P. Luminet, and J.-P. Uzan, Astron. Astrophys. **344**, 735 (1999); H.V. Fagundes and E. Gausmann, Phys. Lett. A **238**, 235 (1998); J.-P. Uzan, R. Lehoucq and J.-P. Luminet, Astron. Astrophys. **351**, 766 (1999); G.I. Gomero, M.J. Rebouças, and A.F.F. Teixeira, Int. J. Mod. Phys. D **9**, 687 (2000); R. Lehoucq, J.-P. Uzan, and J.-P. Luminet, Astron. Astrophys. **363**, 1 (2000); G.I. Gomero, M.J. Rebouças, and A.F.F. Teixeira, Phys. Lett. A **275**, 355 (2000); G.I. Gomero, M.J. Rebouças, and A.F.F. Teixeira, Class. Quantum Grav. **18**, 1885 (2001); G.I. Gomero, A.F.F. Teixeira, M.J. Rebouças and A. Bernui, Int. J. Mod. Phys. D **11**, 869 (2002); A. Marecki, B. Roukema, and S. Bajtlik, Astron. Astrophys. **435**, 427 (2005).

[5] N.J. Cornish, D. Spergel, and G. D. Starkman, Class. Quantum Grav. **15**, 2657 (1998).

[6] M.O. Calvão, G.I. Gomero, B. Mota, and M.J. Rebouças, Class. Quantum Grav. **22** 1991 (2005).

[7] J.-P. Luminet, J. Weeks, A. Riazuelo, R. Lehoucq, and J.-P. Uzan, Nature **425**, 593 (2003).

[8] M.J. Rebouças, J.S. Alcaniz, B. Mota, and M. Makler, astro-ph/0511007. Astron. Astrophys., in press (2006); M.J. Rebouças and J.S. Alcaniz, astro-ph/0603206. Mon. Not. Roy. Astron. Soc., in press (2006); M.J. Rebouças and J.S. Alcaniz, Braz. J. Phys. **35**, 1062 (2005).

[9] A.Y. Kamenshchik, U. Moschella and V. Pasquier, Phys. Lett. B **511**, 265 (2001).

[10] N. Bilic, G.B. Tupper and R.D. Viollier, Phys. Lett. B **535**, 17 (2002).

[11] M.C. Bento, O. Bertolami and A.A. Sen, Phys. Rev. D **66**, 043507 (2002); M.C. Bento, O. Bertolami and A.A. Sen, Phys. Lett. B **575**, 172 (2003); M.C. Bento, O. Bertolami and A.A. Sen, Phys. Rev. D **70**, 083519 (2004).

[12] M.C. Bento, O. Bertolami, M.J. Rebouças, and P.T. Silva, Phys. Rev. D **73**, 043504 (2006).

[13] G.R. Dvali, G. Gabadadze G, and M. Poratti, Phys. Lett. B **485** 208 (2000).

[14] C. Deffayet, Phys. Lett. B **502** 199 (2001);

[15] G. Dvali and M.S. Turner, astro-ph/0301510.

[16] K. Freese and M. Lewis, Phys. Lett. B **540**, 1 (2002).

[17] D.N. Spergel et al., Astrophys. J. Suppl. **148**, 175 (2003).

[18] D.N. Spergel et al., astro-ph/0603449.

[19] R. Aurich, S. Lustig, and F. Steiner, Class. Quantum Grav. **22**, 2061 (2005).

[20] R. Aurich, S. Lustig, and F. Steiner, Class. Quantum Grav. **22**, 3443 (2005).

[21] A.G. Riess et al. [Supernova Search Team Collaboration], Astrophys. J. **607**, 665 (2004).

[22] D. Eisenstein et al., Astrophys. J. **633**, 560 (2005).

[23] J. R. Bond, G. Efstathiou, M. Tegmark, Mon. Not. Roy. Astron. Soc., **291**, L33 (1997); A. Melchiorri, L. Mersini-Houghton, C. J. Odman and M. Trodden, Phys. Rev. D **68**, 043509 (2003).

[24] C. Deffayet, G. Dvali and G. Gabadadze, Phys. Rev. D **65**, 044023 (2002).

[25] C. Deffayet, S. J. Landau, J. Raux, M. Zaldarriaga and P. Astier, Phys. Rev. D **66**, 024019 (2002).

[26] D. J. H. Chung and K. Freese, Phys. Rev. D **61**, 023511 (2000).

[27] P. Gondolo and K. Freese, Phys. Rev. D **68**, 063509 (2003).

[28] A. A. Sen and S. Sen, Phys. Rev. D **68**, 023513 (2003).

- [29] Y. G. Gong and C. K. Duan, Mon. Not. Roy. Astron. Soc. **352**, 847 (2004).
- [30] Z. H. Zhu, M. K. Fujimoto and X. T. He, Astrophys. J. **603**, 365 (2004).
- [31] J.S. Alcaniz and N. Pires, Phys. Rev. D **70**, 047303 (2004).
- [32] M.C. Bento, O.Bertolami, N.M.C. Santos, and A.A.Sen, Phys. Rev. D **71**, 063501 (2005).
- [33] O. Elgaroy and T. Multamaki, Mon. Not. Roy. Astron. Soc. **356**, 475 (2005).
- [34] M. Fairbairn and A. Goobar, astro-ph/0511029.
- [35] R. Maartens and E. Majerotto, astro-ph/0603353.
- [36] Zong-Kuan Guo, Zong-Hong Zhu, J.S. Alcaniz, and Yuan-Zhong Zhang, astro-ph/0603632.
- [37] N.J. Cornish, D.N. Spergel, G.D. Starkman, and E. Komatsu, Phys. Rev. Lett. **92**, 201302 (2004).
- [38] B.F. Roukema et al., Astron. Astrophys. **423**, 821 (2004).
- [39] J. Gundermann, astro-ph/0503014.
- [40] R. Aurich, S. Lustig, and F. Steiner, astro-ph/0510847.
- [41] J. L. Tonry *et al.* [Supernova Search Team Collaboration], Astrophys. J. **594**, 1 (2003).
- [42] B. J. Barris *et al.*, Astrophys. J. **602**, 571 (2004).
- [43] J. Dick, L. Knox and M. Chu, astro-ph/0603247.
- [44] [http://cernlib.web.cern.ch/cernlib/download/2004\\_source/tar/minuit32\\_src.tar.gz](http://cernlib.web.cern.ch/cernlib/download/2004_source/tar/minuit32_src.tar.gz)